

ADA061572

DDC FILE COPY

20 NOV 1978

LEVEL 4

1

9 FIFTH QUARTERLY PROGRESS REPORT. no. 5, 1 Aug-30

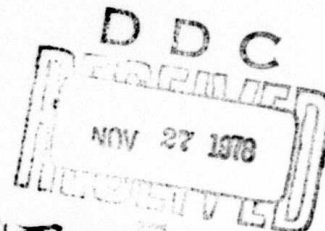
Oct 78

6 LABORATORY APPARATUS FOR THE GENERATION OF RAPIDLY QUENCHED METAL POWDERS

1 August to 30 October 1978

Prepared for:

OFFICE OF NAVAL RESEARCH
ARLINGTON, VIRGINIA 22217



15 Contract No. N00014-77-C-0373, ARPA Order-3363
Start: 01 May 1977
Expiration Date: 31 October 1979

ARPA Order No. 3363
Program Code No. NR-039-141

Principal Investigator:

10 John F. Mahoney,
Julius Perel
Bernard Kalensher
(213) 357-3201

This document has been approved for public release and sale; its distribution is unlimited.

Prepared by:

PHRASOR TECHNOLOGY

1536 Highland Avenue

Duarte, California 91010

78 11 21 020
391 701

Gu

CONTENTS

1.	SUMMARY	1
2.	PROGRESS DURING REPORT PERIOD	2
2.1	SOURCE DEVELOPMENT	2
2.2	FLOW CONTROL	4
2.2.1	EVALUATION OF FEED SYSTEMS	4
2.2.2	VIBRATION FEED SYSTEM TEST	16
2.3	ENGINEERING MODEL	20
2.3.1	CONTROL STATION	20
2.3.2	HEATER CONTROL CIRCUITS	20
2.3.3	HIGH VOLTAGE POWER SUPPLIES	22
2.3.4	TEMPERATURE MEASUREMENT	22
2.4	MATERIALS ANALYSIS	26
2.5	THEORETICAL ANALYSIS	35
2.5.1	RADIATION FROM A MICRON-SIZE CUBICAL BLACKBODY	35
2.5.2	HEAT LOSS SUFFERED BY INSULATED EHD SOURCE	41
	REFERENCES	46
3.	EXPANSION OF THE LABORATORY	47
4.	SPECIAL EVENTS	48
5.	PROBLEMS	48
6.	FISCAL STATUS	48


ILLUSTRATIONS

1.	Exploded View of Vertical Source Components	3
2a.	Pressure Feed System with Feedback	6
2b.	Pressure Feed System with Feedback	6
3.	Oscillating Pressure Feed System	9
4.	Piezoceramic Vibration Feed System	14
5.	Correspondence Between Effective Pressure and Acceleration	15
6.	Effect of Inside Diameter on the Natural Frequency of the Feed System	17
7.	Vibration Feed System Test Setup Showing Vibrator, etc. . .	18
8.	25 kV Isolated Heater Circuit	21
9.	Thermocouple Amplifier Block Diagram	24
10.	Secondary Electron Images of a Splat Cooled Specimen, etc.	27
11.	TEM micrographs of the Splat Cooled Specimen, etc.	29
12.	Electron Diffraction Pattern of the Specimen in Figure 11.	30
13.	Electron Diffraction Pattern of the Specimens, etc. . . .	31
14.	TEM Micrograph of a Second Splat-Cooled Specimen, etc. . .	32
15.	TEM Micrograph of the Specimen in Figure 14 at 75,000X	33
16.	Electron Diffraction Pattern of the Massive Large Grain, etc.	34
17.	Error Incurred in p by Employing Eq. 7 for the Integrals	38
18.	Normalized Power Per Unit Area Radiated, etc.	39

ACCESS IN ()	
NTIS	V. 1/2 Section <input checked="" type="checkbox"/>
DDC	B. 1/2 Section <input type="checkbox"/>
UNCLASSIFIED	<input type="checkbox"/>
BY <i>Per 700</i> <i>50 on file</i>	
DISTRIBUTION/AVAILABILITY CODES	
SPECIAL	
A	

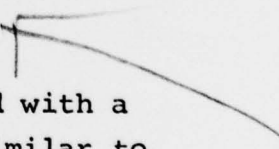
SECTION 1

SUMMARY



The objective of this program is to develop a Table Top Rapid Solidification Powder Generator utilizing electrohydrodynamic (EHD) techniques. EHD is a method of producing very small droplets from a liquid using intense electric fields. The intense field is attained by the application of nominal voltages (several kilovolts) to an emitter having small radius of curvature. When the voltage is applied, the intense field provides sufficient forces upon the liquid surface to form a liquid jet from which droplets are produced. When small droplets are formed from a liquid metal, at the melting point, the droplets will solidify because of heat radiation at rates related to the material properties and the droplet size. The droplet sizes can be varied through a combination of varying the applied voltage and the material mass flow rate. The equipment required to produce metal powders using EHD techniques includes a vacuum system, a droplet source, a particle collector, and the appropriate electronics and test instruments.

During this report period the facility was fitted with a complete machine shop and a new test vacuum chamber similar to the Feasibility Model is under construction. A vertical source was designed and fabricated and is scheduled for testing soon. Various flow control techniques were reviewed and analyzed and an initial test was successfully performed on a vibration feed system. The vacuum system, the cabinets and some components of the Engineering Model were purchased and are scheduled for delivery soon. Electron microscopic analysis of rapid solidification splat cooling showed very fine grain polycrystalline structure with some large single crystals being evident. Theoretical analysis was performed on further studies of radiation from microparticles and source heat shielding techniques were examined.



SECTION 2

PROGRESS DURING REPORT PERIOD

2.1 SOURCE DEVELOPMENT

Design of the vertical microparticle source described in the Fourth Quarterly Progress Report (1 May - 31 July 1978) was completed during this report period. Illustrated in Fig. 1 is an exploded view of the microparticle source showing essential components. Two sources were fabricated and assembled with the exception of the nozzle attachment. Several techniques for affixing the ceramic nozzles to the alumina feed tube are under investigation. The impetus for finding alternative means for joining the nozzle to the feed tube was provided by bench tests indicating that refractory cements may be responsible for spurious currents at high temperature. This aspect of operation is described in more detail below.

A technique for joining nozzles to the alumina feed tube currently investigated involves the electron beam melting of a titanium braze ring at the junction where the nozzle attaches to the feed tube. Under appropriate conditions, titanium has been observed to wet alumina ceramics.

In Fig. 1 the tantalum heater element shown fits into the lower half of the graphite oven (nozzle end). The graphite oven is then subsequently wrapped with alternate layers of molybdenum foil and SAFFIL ceramic paper for heat shielding. This portion of the source is reusable while only the ceramic reservoir (which contains the molten material), feed tube and nozzle are replaced for each test. This source design should allow continuous operation at temperatures near 1400°C.

In addition to unwanted currents observed with ceramic

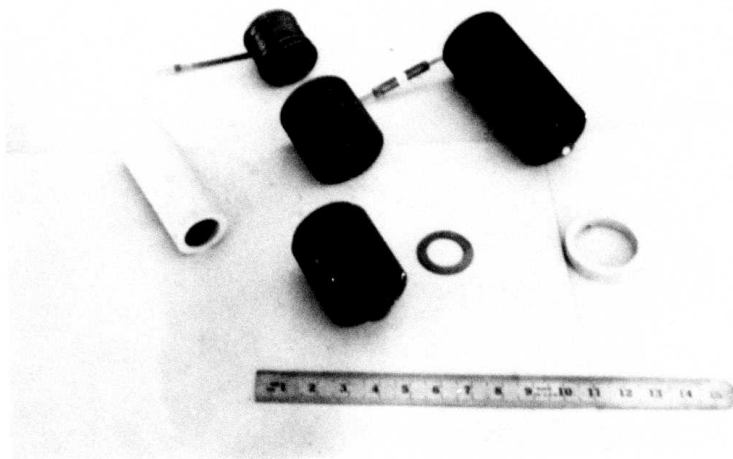


Figure 1 Exploded view of vertical source components.

cements operated at high temperature, similar effects were observed with mullite source components. At temperatures near and exceeding 750°C, large currents originating from these materials were observed upon application of high voltage. A portion of stray currents is attributed to outgassing effects which decrease after a bakeout period. Also a substantial portion of these currents is believed to originate by thermionic ion emission resulting from the alkali impurities present in the refractory cements and mullite components. This phenomenon in fact, has been the basis of ion source development designed to yield a copious supply of alkaline ions at temperatures of 400°C and greater. As a result of measurements in our laboratory, it is concluded that mullite components and refractory cements should be eliminated from further source design. Comparison of stray currents emitted from heated alumina and mullite components indicated that significantly lower currents are observed with alumina components. There is some evidence, although not conclusive, that thermionic emission of electrons from heated and/or contaminated electrodes may be present. This phenomenon is presently under study.

2.2 FLOW CONTROL

2.2.1 EVALUATION OF FEED SYSTEMS

Flow control of the molten material through the nozzle is one of the most important technical problems to be solved at the present time. The generation of controlled size microspheres depends on a well regulated flow of material from the nozzle tip. The least complex feed system would force the flow of the material through the nozzle by means of a static inert gas pressure alone. In order to initiate flow through the nozzle, the pressure has to be high enough to overcome the surface tension of the material at the nozzle exit. After the flow has been established, the pressure differential has to be equal to the pressure drops that

are caused by the flow of the material through the nozzle and/or orifices of the flow passage. The extensive analysis completed previously indicated that for the anticipated flow rates, the pressure drop associated with the flow of the material could only be made equal to the pressure required for overcoming the surface tension at the initiation of the flow. The analysis indicated that this could be accomplished by utilizing a constrictor with a diameter of about 0.001 inch and a length of about 0.5 cm. The incorporation of such a constrictor into the design did not appear to be advisable because of the difficulty of fabricating such a constrictor and the possibility of clogging the small diameter with foreign material. Since the initial pressure difference required for the initiation of the flow could not be dissipated by the pressure drop in the nozzle during flow, the pressure in the feed system had to be decreased immediately after the initiation of the flow. The manual adjustment of the pressure proved to be difficult to achieve.

A task designed to evaluate feed systems based on different principles or a modification of the pressure feed system was therefore initiated. Three systems have been identified as candidates:

- (1) Static pressure feed system with feedback loop
- (2) Oscillating pressure feed system
- (3) Vibration feed system

STATIC PRESSURE FEED SYSTEM WITH FEED BACK LOOP

The pressure feed system with feedback loop is the extension of the original pressure feed system which will incorporate a feedback loop which is designed to maintain a preset pressure differential after the initiation of the flow. The schematic of the system is shown in Figure 2a. The system consists of an inert gas supply whose pressure is regulated by a pressure regulator. Downstream of the regulator is an orifice. The pressure

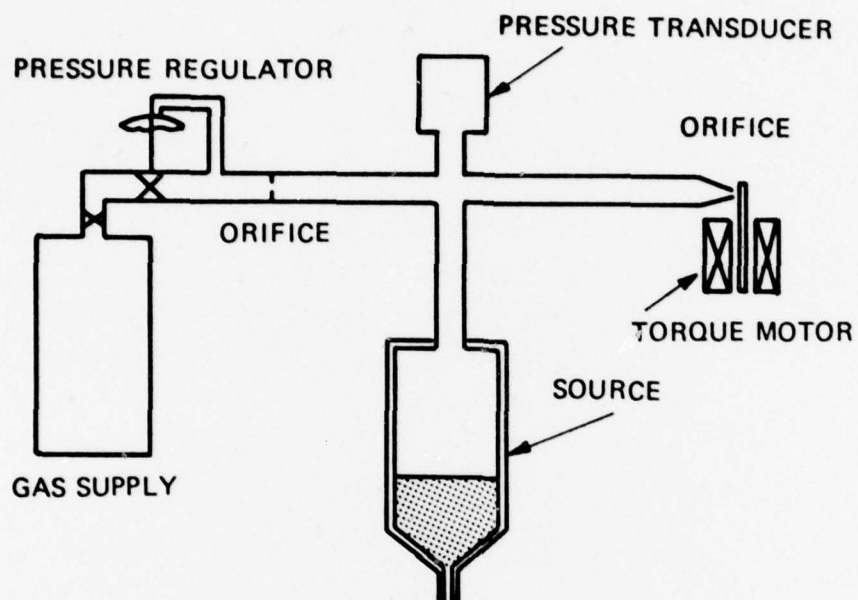


FIGURE 2a PRESSURE FEED SYSTEM WITH FEEDBACK (COMPONENT ARRANGEMENT)

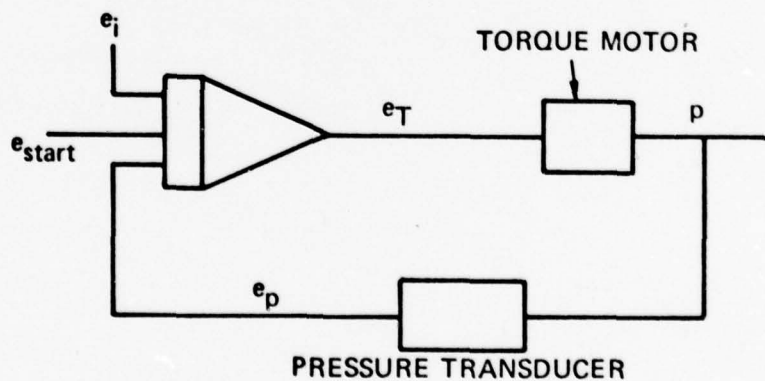


FIGURE 2b PRESSURE FEED SYSTEM WITH FEEDBACK (ELECTRICAL SCHEMATIC)

in the system which is measured by the pressure transducer is determined by the size of the orifice nearest the torque motor. The flow coefficient of this orifice is determined by the position of the flapper of the torque motor. The torque motor would be driven by the output of an operational amplifier whose input is an initial voltage and the voltage output of the pressure transducer as feedback. An initial voltage spike into the operational amplifier would cause the flapper to be seated momentarily for raising pressure within the system to the level required for initiating the flow. The schematic of the feedback loop is shown in Figure 2b.

The response and stability of the system depends on the various parameters of the system, the flow rate, the volume, the gas pressure and the size of the two orifices.

The system has two disadvantages which make it less desirable to implement. The system requires a continuous flow of inert gas. Since the gas pressure in the system is less than atmospheric, the gas flow issuing from the flapper valve would have to be vented into a vacuum. It has the advantage of feeding the material by the most direct method without movement or vibration of critical components.

This system will not be pursued at this time because one of the other two candidate systems was selected for hardware study.

OSCILLATING PRESSURE FEED SYSTEM

The oscillating pressure feed system is an extension of the feed system discussed above as it still employs pressure as the driving force for moving the material through the nozzle. But instead of forcing the flow by a steady pressure, the flow is adjusted by the periodic increase of the pressure whose frequency and magnitude can be adjusted electrically with ease.

The basic pressure oscillating feed system is shown in Figure 3. The system consists of metal bellows which is enclosed in a volume in such a fashion that a small movement of the bellows flange will result in a relatively large change of the total gas volume of the system. The short pressure fluctuations will overcome the surface tension at the tip of the nozzle and initiate the flow of the material. The spring is required to position the flange of the bellows under steady state conditions when the external pressure will be higher than the internal pressure. Without the spring, the flange would be seated on the bottom of the variable volume under steady state conditions.

The flange of the bellows is driven by a vibrator whose frequency and stroke can be adjusted electrically over a wide range.

The total volume of the gas in the system is

$$V_T = V_1 + V_2 + V_3 \quad (1)$$

where V_1 volume of reservoir
 V_2 volume of tube
 V_3 volume of variable volume.

The change in volume V_T with the displacement of the flange of the bellows is

$$dV = d(V_1 + V_2 + V_3) \quad (2)$$

$$dV_T = dV_3 \quad (3)$$

$$dV_T = \frac{D^2 \pi}{4} dx' \quad (4)$$

where D is the diameter of the flange and x' is the flange position.

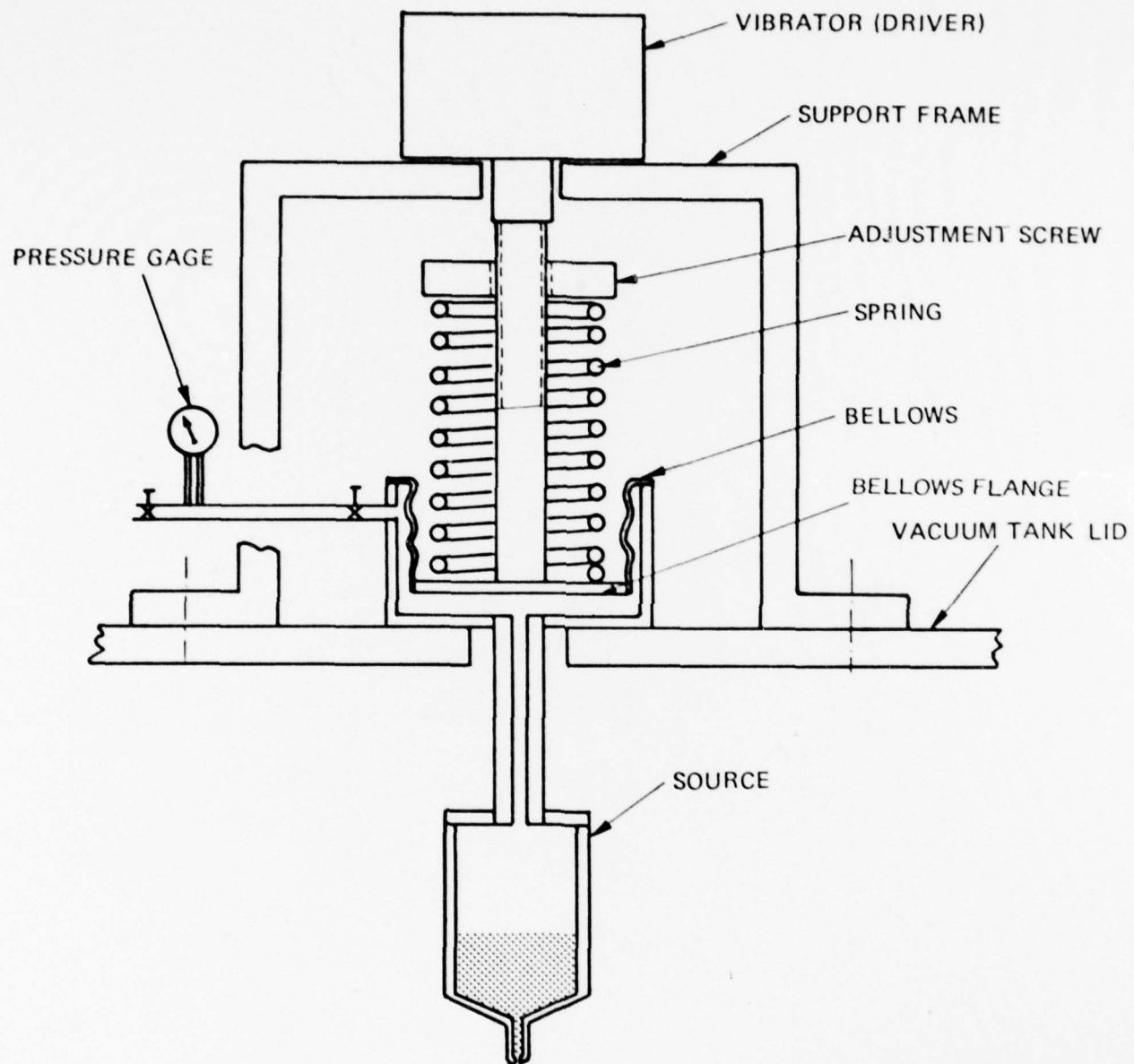


Figure 3 Oscillating Pressure Feed System

Since it will be assumed that the frequency is relatively high, that no effective heat transfer will take place and that therefore the expansion and compression of the gas in the volume occurs adiabatically, the relation between pressure and volume is then given by

$$pV^\gamma = \text{constant}. \quad (5)$$

By differentiation of relation (5)

$$V^\gamma dp + p\gamma V^{\gamma-1} dV = 0. \quad (6)$$

Relations (6) can be solved for the change in pressure, i.e.,

$$dp = -\frac{\gamma p}{V} dV. \quad (7)$$

When the change of volume of relation (4) is inserted in relation (7)

$$dp = \frac{\gamma D^2 \pi}{4V} dx'. \quad (8)$$

Under steady state conditions the force on the flange is zero, i.e.,

$$F = 0, \quad (9)$$

where

$$F = (p_a - p_o)A - k\ell, \quad (10)$$

p_a = ambient pressure

p_o = internal pressure

A = area of flange

k = combined spring constant of spring and bellows

ℓ = initial stretch of spring and bellows

Differentiation of relation (10) gives

$$\Delta F = A \Delta p_O - k \Delta t. \quad (11)$$

When the change of pressure is replaced by relation (8) and replacing the change of spring extension by the movement of the flange, dx , and dividing by the differential displacement, the effective spring constant of the system is found,

$$\left| \frac{\Delta F}{\Delta X'} \right| = k' = \frac{P_O \gamma}{V_T} \left(\frac{D^2 \pi}{4} \right)^2 + k, \quad (12)$$

where k' is the effective spring constant.

The natural frequency of the system is

$$f = \frac{1}{2\pi} \left(\frac{k'}{m} \right)^{1/2} \quad (13)$$

By inserting the effective spring constant of relation (12), the natural frequency of the system is found to be

$$f = \frac{1}{2\pi} \left[\frac{P_O \gamma}{V_T m} \left(\frac{D^2 \pi}{4} \right)^2 + \frac{k}{m} \right]^{1/2} \quad (14)$$

The lowest natural frequency is achieved by selecting a spring and bellows combination with a very small combined spring constant k .

For a typical case where

$\gamma = 1.63$ (argon)	$D = 3$ in
$p_O = 10$ psia	$V_T = 2.4$ in ³
$g = 32.2$ ft/sec ²	$W = 0.25$ lb

the natural frequency is

$$f = 115 \text{ Hz}$$

The natural frequency can be increased by increasing the spring constant though the spring constant k cannot be greater than

$$k < \frac{D^2 \pi}{4a} (p_a - p_o) \quad (15)$$

where a = half amplitude of the movement of the flange.

If the diameter of the tube that connects the variable volume with the volume in the reservoir is small, the effect of damping of the pressure wave emanating from the variable volume has to be taken into account. The advantage of the oscillating pressure feed system lies in the ease with which the feed can be controlled by variations in the electrical input to the driver. The main components of the system remain stationary and are not subjected to vibration and periodic high acceleration forces. By making the variable volume, V_3 , relatively large in comparison to the volume of the reservoir, V_1 , and maintaining the steady state pressure constant, the feed rate can remain constant from the beginning to the end of the operation during which the entire material in the reservoir is expelled without making adjustments to the driver.

VIBRATION FEED SYSTEM

The vibrating feed system employs the pressure generated by the acceleration on the material in the reservoir to overcome the surface tension at the tip of the nozzle. The acceleration force can also be employed for overcoming the pressure drop due to the flow of material if the feed system is operated without inert gas pressure. Since the pressure drop due to the flow through the nozzle is much smaller than the pressure differential established by the surface tension, it would be possible to operate the feed system with the reservoir vented to the vacuum and regulate the flow entirely by the forces generated by the vibration of the retort.

A design of this type feed system is shown in Figure 4. The feed system is suspended from a relatively stiff retainer structure which is bolted to the vacuum flange. The tube on which the reservoir is suspended is fed through the vacuum flange by metal bellows. Two piezo-electric crystals are clamped against the retainer by a nut which is threaded on a sleeve which is part of the suspension rod of the retort. By exciting the piezo-electric crystals the reservoir is subjected to forced vibration.

The acceleration (a) that is experienced by the retort and the material in it is a function of the frequency (f) and the half amplitude (B) of the vibration of the reservoir, i.e.,

$$a = \omega^2 B$$

where $\omega = 2\pi f$.

The least amount of driving force will be required for causing the source to vibrate at a relatively large amplitude required for the desired acceleration when the feed system vibrates at its natural frequency.

In Figure 5 the correlation between effective pressure and acceleration are presented. It can be seen that for aluminum which has been filled to a height of 2 cm in the reservoir and which has to exit through a nozzle throat of 0.003 in diameter, a pressure of 6.4 psi has to be applied to overcome the surface tension. The pressure can be generated with an acceleration of 1.11×10^5 in/sec² or 290g.

The relation between acceleration, amplitude and frequency indicates that in order to minimize the movement of the source, i.e., hold the amplitude to a minimum, the frequency should be as high as possible. This consideration would indicate the requirement for a system which is very stiff. This can be achieved by making the tube from which the source is suspended

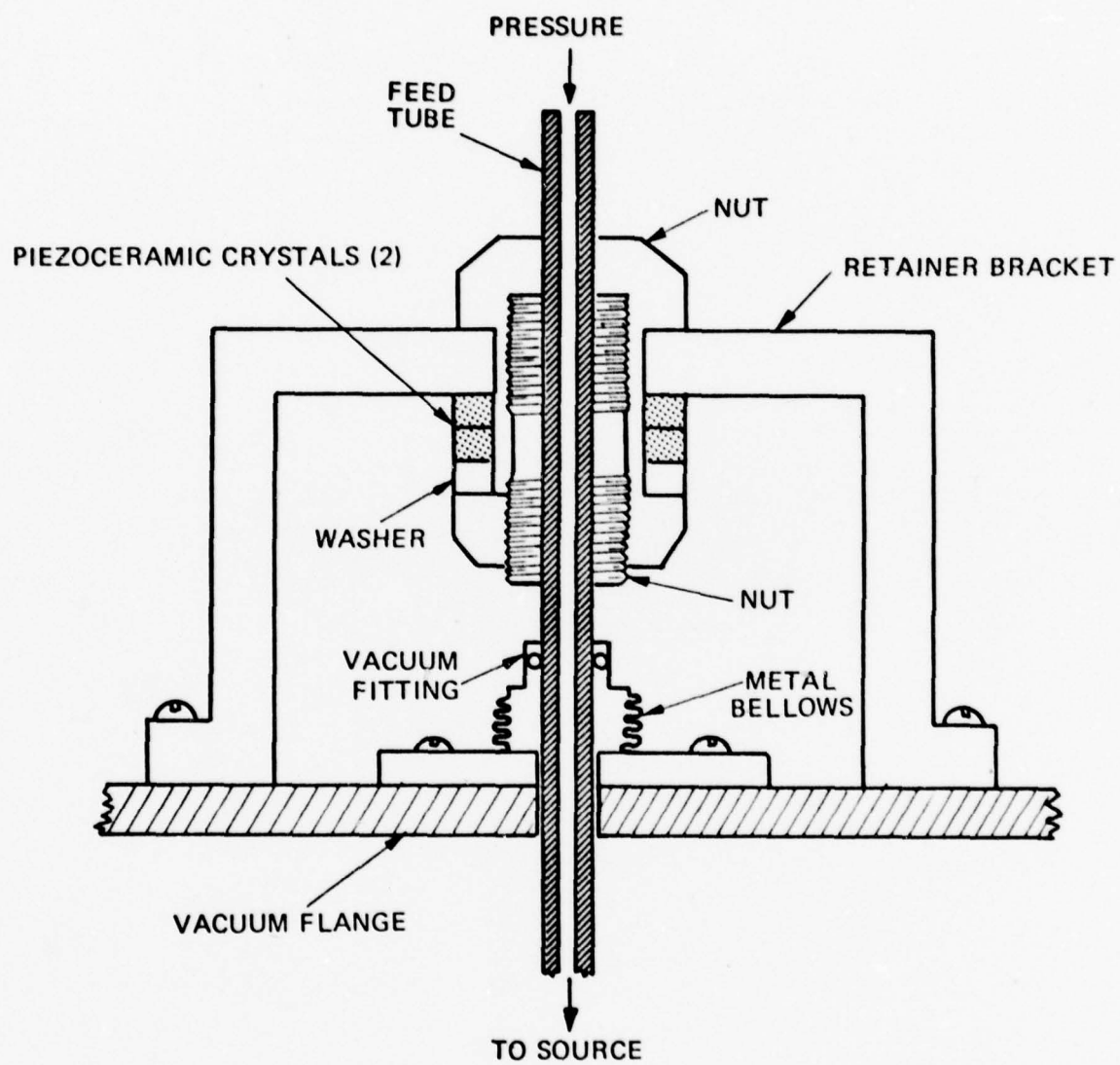


Figure 4 Piezoceramic Vibration Feed System

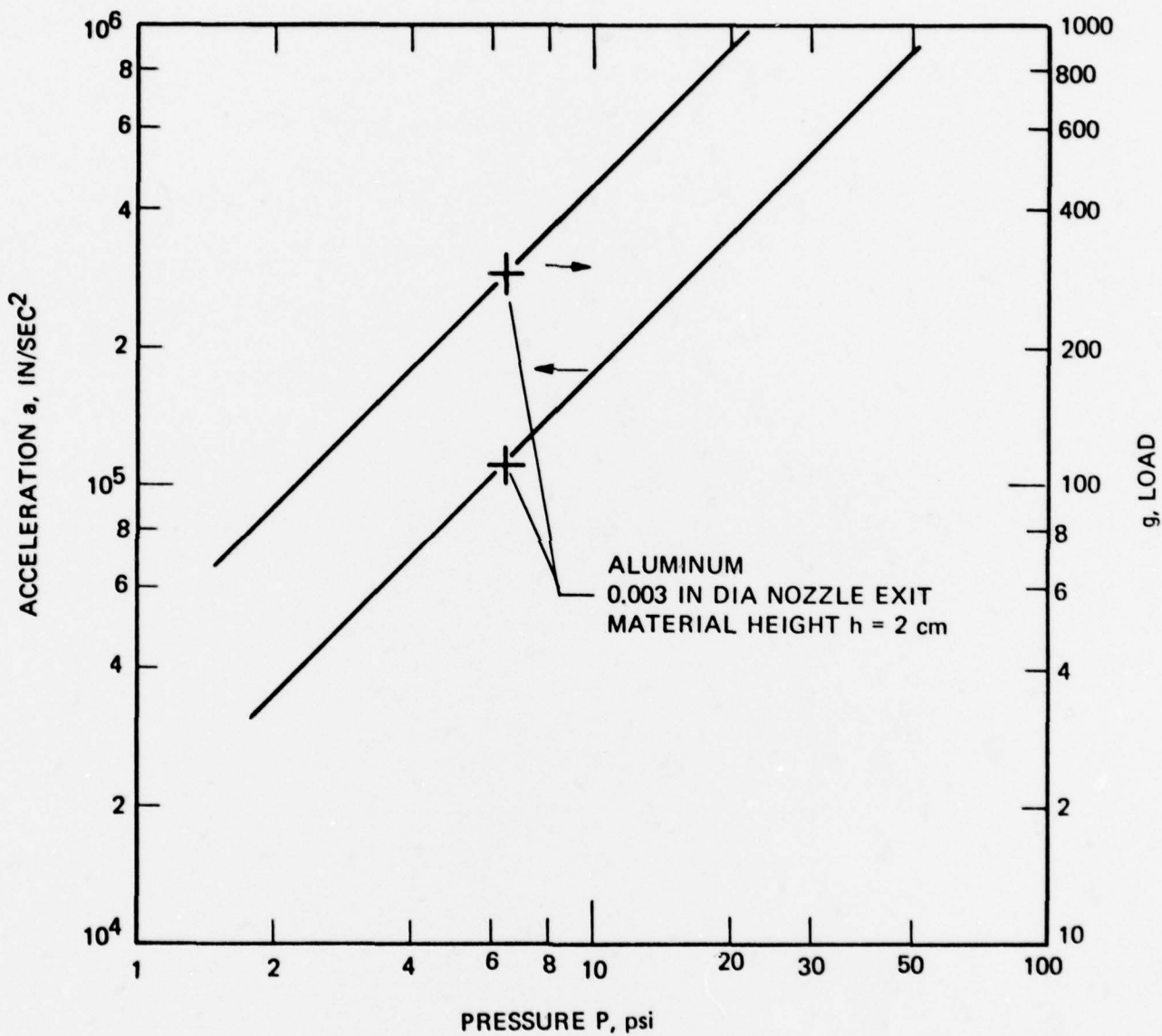


Figure 5 Correspondence Between Effective Pressure and Acceleration

with a very large outside diameter and only a very small inside diameter. This type of suspension is not recommended by the thermal design which attempts to minimize the heat flow from the source.

In Figure 6 the effect of the inside diameter of a quarter inch outside diameter tube on the natural frequency of the system is presented. The frequency approaches an upper value of about 2100 Hz. At that frequency the required amplitude would be 1.4×10^{-3} inch. If the system is entirely undamped, the system cannot be forced at its natural frequency since it would destruct itself. The required acceleration would be achieved at a slightly lower frequency and higher amplitude.

From the analysis it can be seen that the forcing frequency has to be adjusted during the operation of the system to account for the decrease of the materials level in the reservoir. In order to maintain a constant flow rate the forcing frequency has to be increased with time. The exact time dependence could be established after the operation of the feed system has been experimentally verified.

2.2.2 VIBRATION FEED SYSTEM TEST

A bench test of vibration feed system was made using a setup similar to that design described in the previous subsection. Instead of using piezoelectric drivers to provide the vibration a commercial vibrator was used.

Figure 7 shows the vibrator mounted on top of a vacuum chamber flange. The figure also shows the vertical feed tube which conducts both the gas feed pressure and the mechanical vibration to the droplet source at the end. The source contains the liquid metal and the capillary needle nozzle where the metallic droplets are formed. In the present bench test mercury was used because, as in the case of many liquid metals

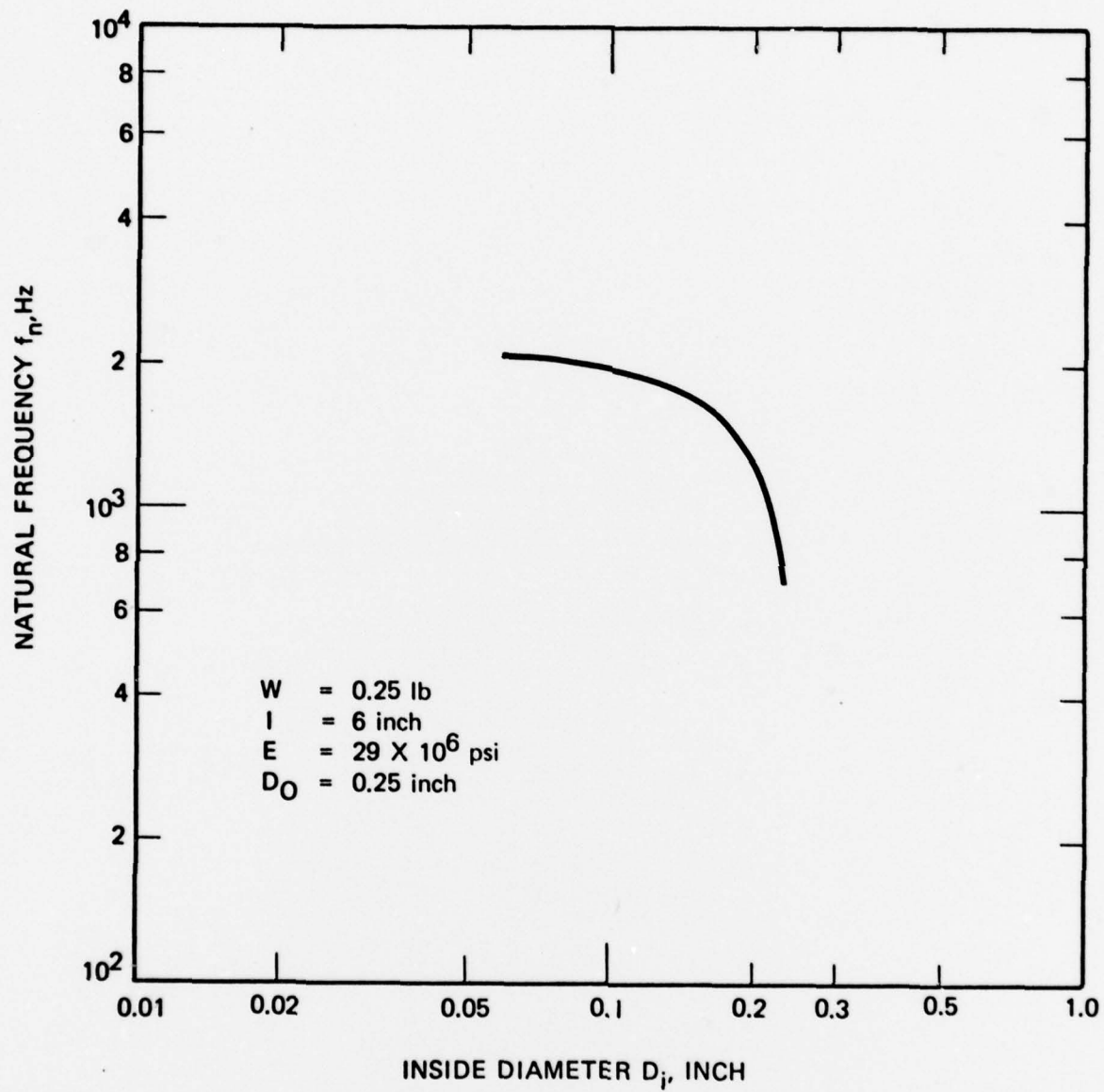


Figure 6 Effects of Inside Diameter on the Natural Frequency of the Feed System

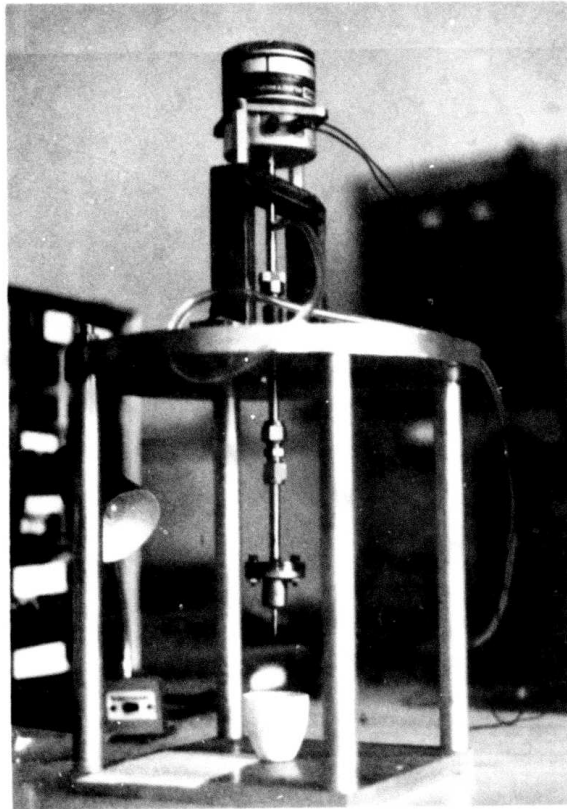


Figure 7 Vibration Feed System Test Setup showing vibrator, pressure delivery tubing and nozzle.

in contact with ceramic sources, the liquid is non wetting. The vibrator shown in Fig. 7 consists of a steel body with a center pole accurately located in the center of the top ring so that a uniform air gap is obtained. This eliminates any initial setting up procedures or subsequent adjustments during the operational life of the vibrator. A moving coil is located in the annular gap by means of flexible suspension units. This enables the AC coil to produce axial motion of the lightweight moving table without undue restraint from the suspension units, particularly at low frequencies when the excursion is a maximum.

The vibrator functions by means of the interaction between the magnetic field in the air gap and the oscillating current flowing in the moving coil. This current generates a force which is proportional to the product of the instantaneous current and the magnetic flux density. The driving current is obtained from a power amplifier which is controlled by a variable frequency oscillator not shown in the figure. The frequency and amplitude of the vibrator are controlled by and are proportional to the oscillator signal fed to the amplifier.

Preliminary results indicate that, at resonant frequencies, a vibration system is able to drive the mercury through the 0.004 inch nozzle with no gas pressure differential in the feed system. For the particular configuration tested this occurred at a frequency of 400 Hz. At other frequencies, combinations of pressure and vibrations at various amplitudes produced liquid flow.

The primary aim of this test was to demonstrate that vibration could enhance the flow of a non wetting liquid through a narrow orifice and aid in the control of this flow. This was indeed demonstrated and therefore opened a new direction of flow control. The required frequency and amplitude will depend upon the particular configuration of source and feed system. It yet remains a question whether the oscillating pressure or the mechanical vibrator is superior for feed control.

2.3 ENGINEERING MODEL

2.3.1 CONTROL STATION

The basic Engineering Model system including cabinets, instrumentation, pumping station, valving and controls was purchased during this report period. Delivery of this first unit is expected in early December. Final design features of the engineering model chamber are awaiting completion of Feasibility Model tests which will further define the chamber specifications.

2.3.2 HEATER CONTROL CIRCUITS

Heater control for the microparticle source reservoir and nozzle in the Feasibility Model have utilized manually controllable variacs isolated from the high voltage portion of the system. Isolation is provided by high voltage step-down isolation transformers. Several alternative control systems for the Engineering Model are being examined. One method under consideration would not differ significantly from the Feasibility Control but would add the feature of motorizing the variac. The motor chosen for this function would be selected on the basis of operating on command via a programming voltage output signal from the Engineering Model computer.

A second technique for the 25kV isolated heater control circuit uses a 250 watt power amplifier to provide the heater current in the primary side of a step-down isolation transformer. The input signal to the amplifier is controlled by a heater programming voltage as indicated in the block diagram illustrated in Fig. 8. This type of approach has several advantages over the previously discussed method. First of all, no moving parts are involved and control circuits are less complex than those required in the motorized case. It is planned to use a general purpose audio amplifier in the Engineering Model.

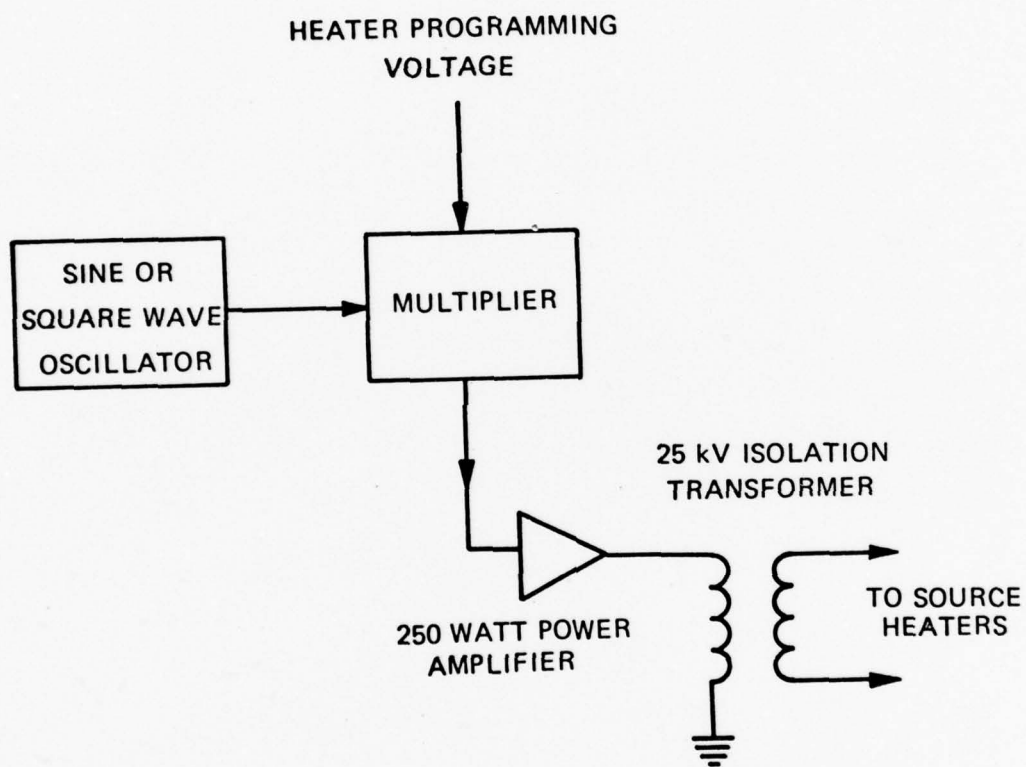


Figure 8 25 kV Isolated Heater Circuit

This component could be greatly simplified in function and cost for the Prototype System by utilizing a custom designed power amplifier. Ultimately a single frequency or a very narrow frequency band is all that is required.

2.3.3 HIGH VOLTAGE POWER SUPPLIES

The high voltage power supplies for operation of the source, extractor and lens in the Engineering Model have been ordered and delivery is expected sometime in December, 1978. These supplies have special features including:

- o Remote Voltage Programming

This enables the power supply to be controlled by an external low voltage DC signal source from a computer.

- o Floating Ground

This feature isolates the "low end" return of the power supply with respect to ground.

The first feature is required for automated control capability in the Engineering Model. The second option allows the user to monitor the load current with accurate instrumentation such as an appropriate milliammeter or microammeter measuring device.

2.3.4 TEMPERATURE MEASUREMENT

In the laboratory Feasibility Model, temperature monitoring instrumentation floats at the high potential applied to the microparticle source. Thus the system user must be protected against coming into physical contact with the measuring devices. Also, this arrangement limits operations such as range switching, etc.

In order to eliminate the hazards of floating instrumentation and increase the versatility of the temperature

monitoring instrumentation, the Engineering Model will permit thermocouple and other appropriate signals to be measured by meters at ground potential. Thus a circuit design to accomplish this objective was initiated and completed during this report period. This design was necessary as no commercially available instrument that fulfills the isolation requirements for the Engineering Model is presently available on the market.

The description which follows deals only with thermocouple measurements but similar circuits will be developed as required for additional signals.

GENERAL DESCRIPTION

The thermocouple amplifier accepts a low level signal from a thermocouple or other millivolt source, provides amplification signal conditioning, isolation and linearization. An analog output voltage is provided that linearly represents the measured temperature. The amplifier features 20 kilovolt common mode voltage rejection capabilities and a selection switch so that either type K (Alumel Chromel) or type C (Tungsten 6% Rhenium, Tungsten 26% Rhenium) thermocouples can be used. The calibrated output is linear and produces one millivolt per degree C measured. A buffered analog output voltage is provided which may be utilized to drive a strip chart recorder. The high voltage isolation characteristics are obtained by frequency modulating the analog signal and transferring it across an air gap utilizing an infrared emitter and photo-detector. Referring to the block diagram of Figure 9, a general description of the amplifier follows.

The input signal is applied to a stable, precision amplifier with a low temperature coefficient of offset drift. This amplifier (A1) amplifies the thermocouple signal to a level of approximately one millivolt per degree input. A 0°C cold reference junction is included in the circuit that compensates for the junction formed by the thermocouple wire connections

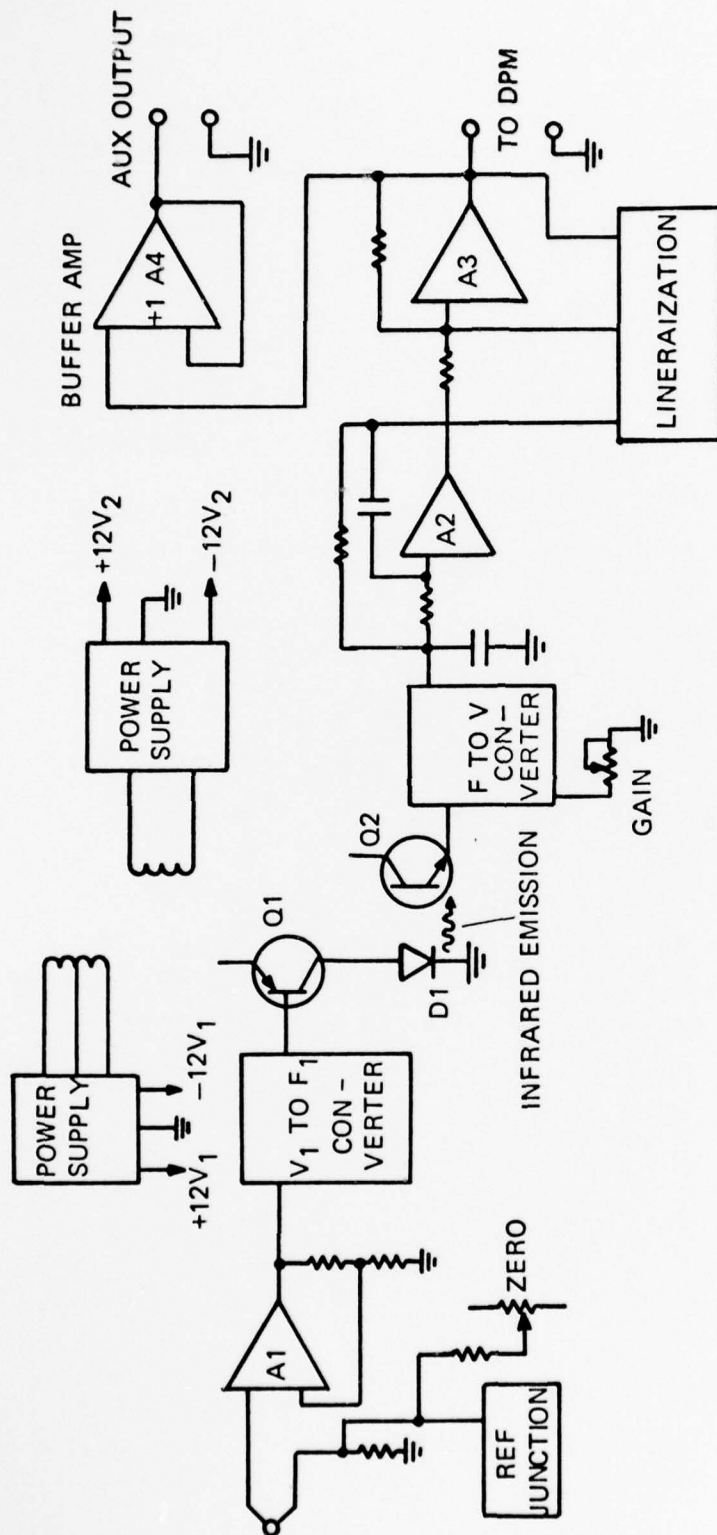


Figure 9 Thermocouple Amplifier Block Diagram

to the amplifier input. The amplified analog signal is applied to the input of a voltage-to-frequency converter whose output is 6.667 Hz per millivolt (= 1 degree C) input. The frequency output of the V to F converter drives a current switch, Q1, that provides approximately 50mA current pulses to the infrared emitting diode, D1. An input zero control is provided that removes all the offset voltages referred to the input of the amplifier in addition to compensating for any offset in the V to F converter. (A scaling adjustment and output zero controls are provided in the output section of the amplifier). Power is supplied to this isolated input section of the amplifier by a winding on a power transformer whose breakdown voltage is in excess of 20 kilovolts. Regulated voltages are supplied by a dual plus and minus 12V regulator. The input section is totally isolated from power lines, earth ground and the output section. It also has the capability to "float" to positive or negative potentials in excess of 20 kilovolts with respect to the output section or earth ground.

The frequency modulated pulses emitted by the infrared light emitting diode are sensed by a photodetector transistor, Q2, connected in tandem with a common base configuration of PNP transistor amplifier to maximize the system's frequency response. The amplified pulses are applied to a frequency-to-voltage converter whose nominal output is one millivolt per 6.667 Hz input. An output of one millivolt from the F to V converter represents approximately one degree C of the measured temperature. The current output pulses of the F to V converter are filtered by the two pole filter comprised of A2 and its associated components.

Linearization for types C and K thermocouples is accomplished at amplifier A3 and the switchable linearization components. Linearization is accomplished utilizing five segment approximation for the desired nonlinear curves. Gain and offset adjustments are made at amplifier A3 at each

linearization break point. The linear output of A3, one millivolt per $^{\circ}\text{C}$, is applied to a digital panel meter whose sensitivity is one digit (degree) per millivolt. The full scale capabilities of the system (maximum accuracy) are 1350°C for type K, chromel-alumel, thermocouple and 1650°C for type C, tungsten-5% Rhenium - tungsten - 26% rhenium, thermocouples.

Amplifier A4 is a gain of +1 buffer amplifier providing an auxiliary output that may be used to drive a strip chart recorder.

2.4 MATERIALS ANALYSIS

Analysis of Al-4.5% Cu Alloy Splats

One of the aims of this program is to demonstrate the capability of the EHD apparatus to produce rapidly solidified splats of alloys on various substrates. In a number of experiments performed to date, splats of Al-4.5% Cu alloy were produced on substrates of copper, aluminum and Vinyl Cellulose and were examined by electron microscope techniques.

Figure 10 shows secondary electron images of a splat cooled Al-4.5% Cu alloy specimen produced on a copper substrate as viewed perpendicular to the substrate surface. The figure shows that the substrate was uniformly coated by successive impinging liquid metal droplets. While individual splats are clearly distinguishable on the specimen surface, no distinction could be made when the cross section of the splats were examined - successive droplets were welded together in a manner similar to classical splat cooled specimens. Furthermore, cross sectional views of the splats in the SEM at magnifications of up to 10,000X did not reveal a clearly distinguishable microstructure. TEM studies were thus undertaken at higher magnifications.

**Best
Available
Copy**

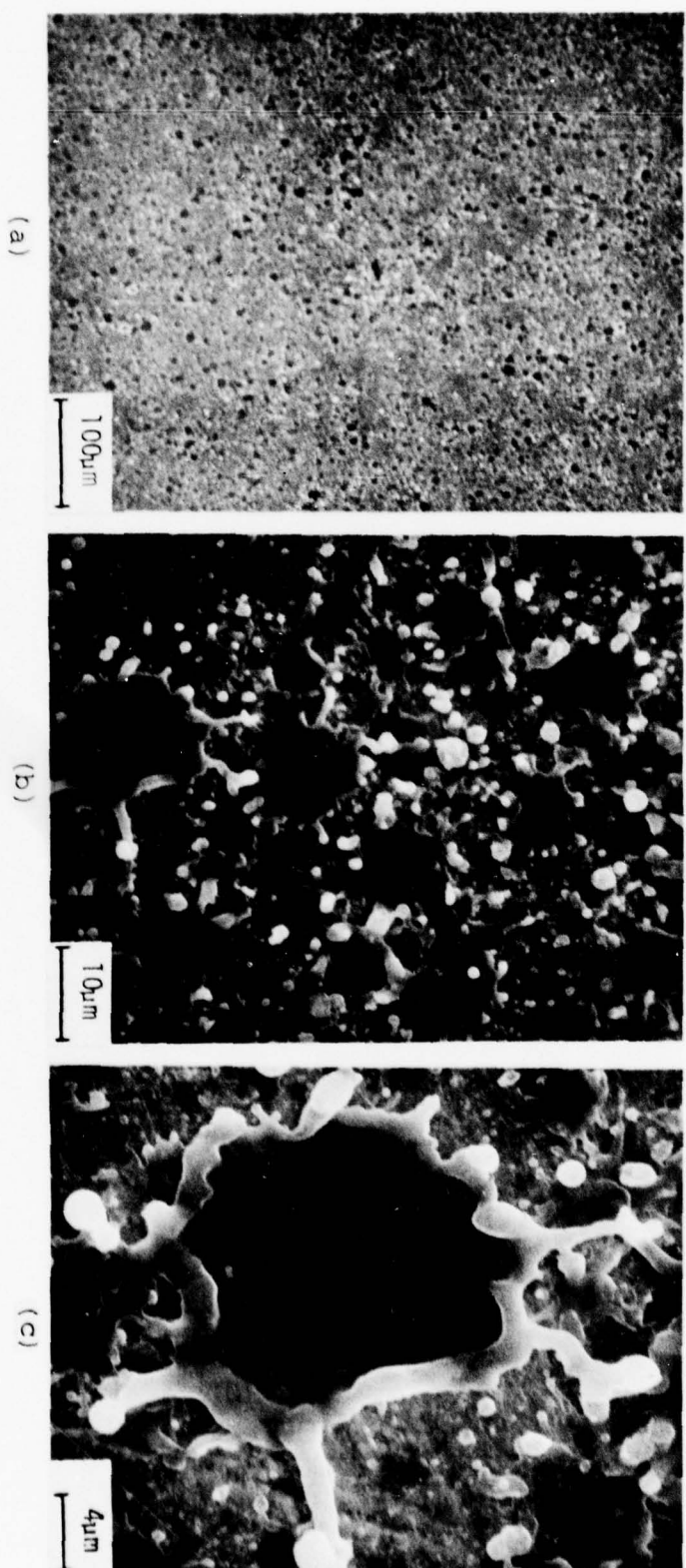


Figure 10 Secondary Electron Images of a sputter cooled specimen of Al-4.5% Cu alloy produced in the EHD apparatus on a copper substrate; (a), (b) and (c) show views of the sputter surface at 100X, 1000X and 2500X, respectively.

Splats of the Al-4.5% Cu alloy produced on copper substrates contained some electron transparent regions. These were analyzed by conventional TEM and electron diffraction.

Figure 11 shows a TEM micrograph of a portion of a splat at 75,000X. The specimen is composed of very fine grains as evidenced by the electron diffraction pattern in Figure 12. Figure 13, which is the electron diffraction pattern of the large dark area in Figure 11, shows again the multigrained (polycrystalline) nature of the splat. One crystal orientation can clearly be discerned in this pattern.

A second area of the splat was examined, Figures 14 and 15. The structure looks cellular, however, it may be due to surface markings of the substrate material. The electron diffraction pattern of the large grain shows it to be a single crystal, Figure 16.

In general, the grain size of these splat cooled specimens are in the range of $\sim 0.025\mu\text{m}$ to $\sim 0.13\mu\text{m}$. Previous investigators have reported the occurrence of both equiaxed and columnar grains in aluminum alloy splats (Ref. 1). Grain sizes in these splat-cooled specimens are normally within the range of 0.1 to $10\mu\text{m}$. However, grain sizes as small as $0.01\mu\text{m}$ have been reported in electron-transparent regions of splat-cooled foils of Al-33% Ge alloy (Ref. 2).

It is tempting to try and correlate the observed grain size in these specimens to cooling rate during solidification. Recently, an attempt was made to develop a formal theory of transformation kinetics coupled with classical nucleation and growth theories for this purpose (Ref. 3). However, the predicted values of grain size in massively solidified alloys are in variance with experimental observations, including those of the present investigation.



Figure 11 TEM micrographs of the splat cooled specimen of Al-4.5% Cu alloy shown in Figure 10. Magnification: 75,000X.

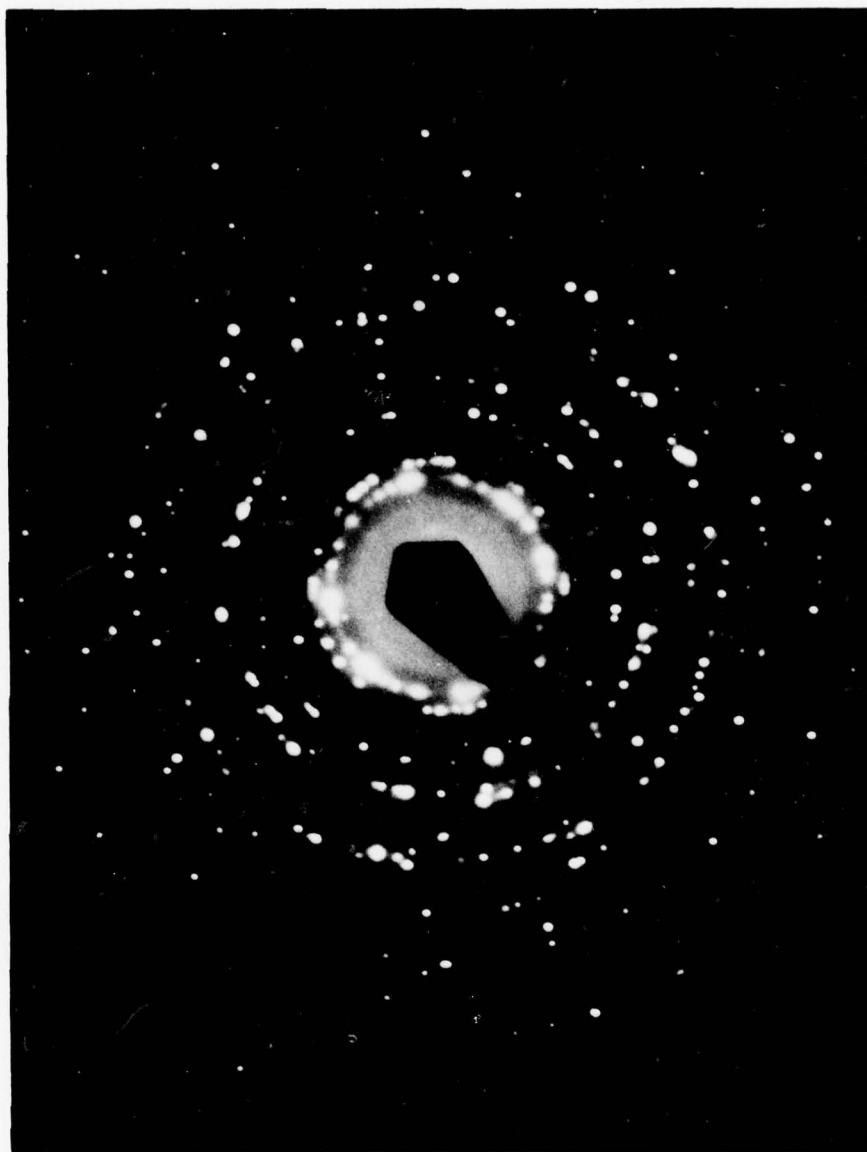


Figure 12 Electron Diffraction pattern of the specimen in Figure 11 indicating the multi-grain nature of the splat.

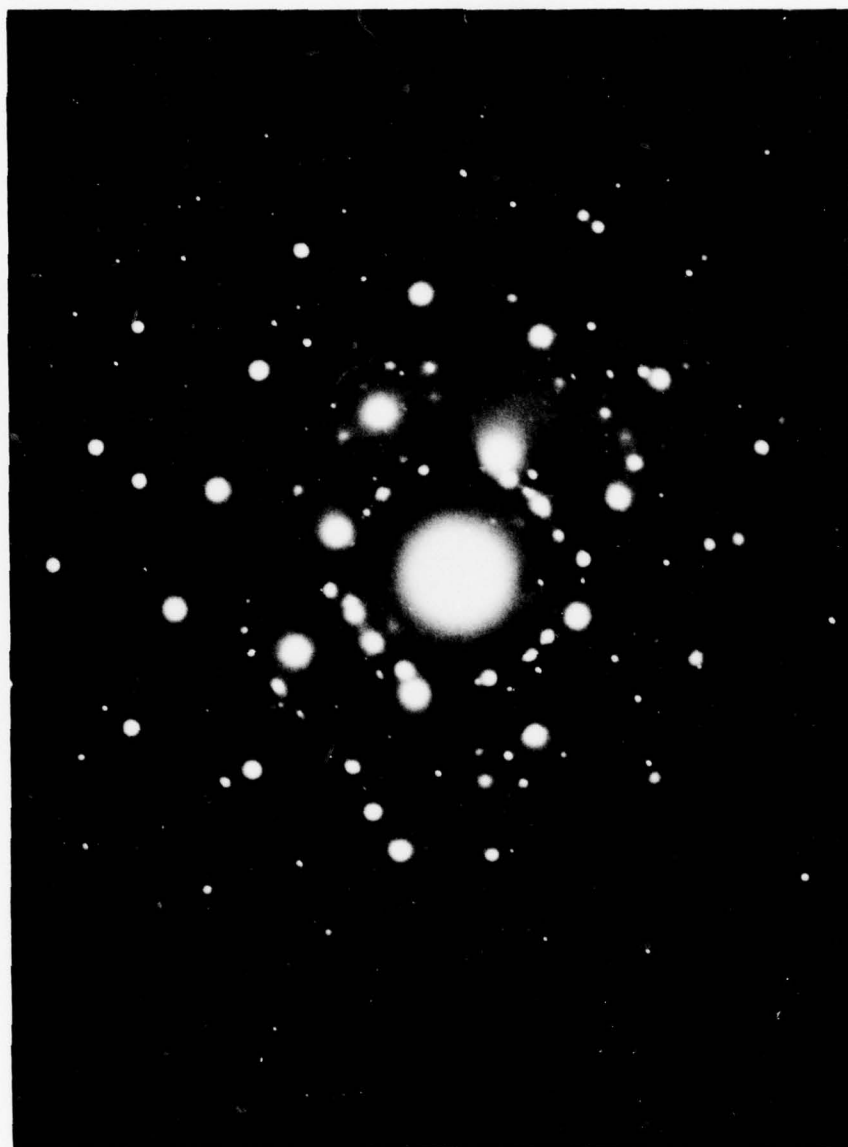


Figure 13 Electron Diffraction pattern of the specimens in Figure 11 in the region of the large dark grain.



Figure 14 TEM micrograph of a second splat-cooled specimen of Al-4.5%
Cu alloy splat produced on a copper substrate. Magnification: 30,000X.

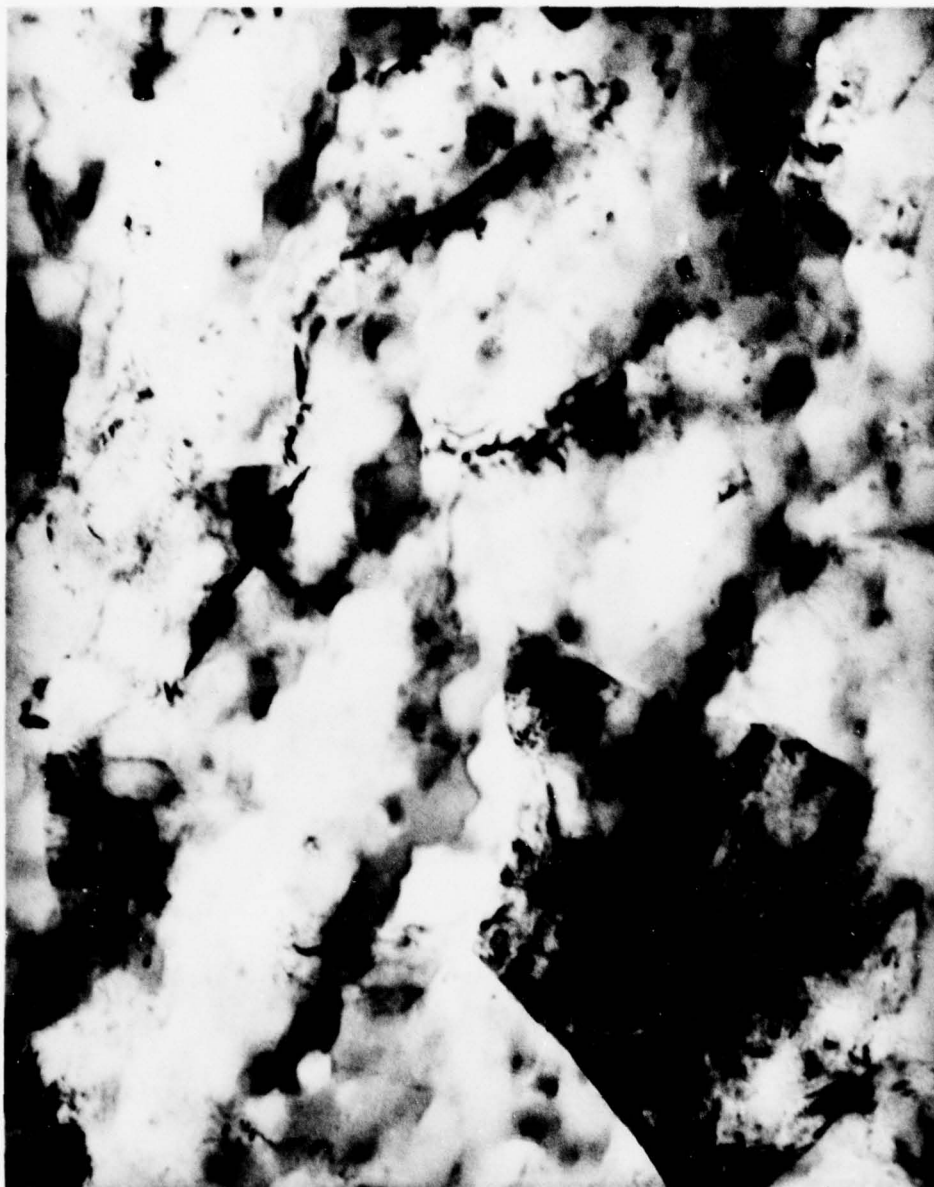


Figure 15 TEM micrograph of the specimen in Figure 14 at 75,000X.



Figure 16 Electron Diffraction pattern of the massive large grain in Figure 15.

In summary then, a second important capability of the EHD apparatus to produce controlled thickness, rapidly solidified, splats has been demonstrated with Al-4.5% Cu alloy. The structures obtained are at the finer range of those reported in splat-cooled specimens via conventional techniques.

2.5 THEORETICAL ANALYSIS

2.5.1 RADIATION FROM A MICRON-SIZE CUBICAL BLACKBODY

The familiar Stefan-Boltzmann radiation law, given by

$$P = \sigma T^4 \quad (16)$$

where, $\sigma = 5.67 \times 10^{-8}$ watts/(m² °K⁴) and T = temperature of the black surface, is valid only for blackbodies that are large compared to the emitted wavelengths. If the blackbody is of the order of a micron in size, then Eq. 16 no longer correctly describes the radiated power. A modified Stefan-Boltzmann radiation law for a micron-size, cubical blackbody was presented previously (Fourth Quarterly Progress Report Eq. 8, p.15). This expression, however, is only approximate, since the spectral intensity $P_\nu d\nu$ (= power radiated per unit area of a black surface in the frequency interval $\nu, \nu + d\nu$) was integrated over all frequencies, instead of over the allowed frequencies, which simplified the task of integration. It was shown that

$$P_\nu d\nu = \left(\frac{2\pi\nu^2}{c^2} - \frac{\beta_1\nu}{4c\ell} - \frac{\beta_2}{4\ell^2} \right) \frac{h\nu d\nu}{\exp\left(\frac{h\nu}{kT}\right) - 1} \quad (17)$$

where, ℓ = side of the cube, c = velocity of light, h = Planck's constant, k = Boltzmann's constant and $\beta_1 = 19.6324$, $\beta_2 = 12.7385$. Since it must be true that $P_\nu d\nu \geq 0$, therefore, from Eq. 17, the frequency ν must satisfy

$$\nu \geq \frac{3.608 \times 10^8}{\ell}, \text{ sec}^{-1} \quad (18)$$

where ℓ is expressed in meters. Thus, the allowed frequencies are defined by Eq. 18. Let ν_0 denote the minimum allowed frequency, i.e., let

$$\nu_0 = \frac{3.608 \times 10^8}{\ell}, \text{ sec}^{-1}.$$

Then, the power radiated per unit area over all the allowed frequencies is

$$P = \int_{\nu_0}^{\infty} P_{\nu} d\nu \quad (19)$$

where $P_{\nu} d\nu$ is given by Eq. 17. Thus,

$$P = \frac{2\pi h}{c^2} I_1 - \frac{\beta_1 h}{4c} \frac{I_2}{\ell} - \frac{\beta_2 h}{4} \frac{I_3}{\ell^2} \quad (20)$$

where

$$I_i = \int_{\nu_0}^{\infty} \frac{\nu^{4-i} d\nu}{\exp\left(\frac{h\nu}{kT}\right) - 1} \quad (i = 1, 2, 3)$$

It can be shown that the integrals I_i are given by

$$I_i = \left(\frac{kT}{h}\right)^{5-i} \left\{ \alpha^{4-i} \ln(1-e^{-\alpha})^{-1} + (4-i)! \sum_{n=1}^{\infty} \frac{e^{-n\alpha}}{n^{5-i}} \left[(3-i)(2-i) \frac{n^2 \alpha^2}{4} + \frac{(3-i)}{(3-i)!} n\alpha + 1 \right] \right\} \quad (21)$$

where, $i = 1, 2, 3$ and, $\alpha = \nu_0 h/kT$. Note that $0! = 1$, by definition.

Eqs. 20 and 21 represent the correct, modified Stefan-Boltzmann radiation law for a micron-size, cubical blackbody. When ℓ becomes large, so that both ν_0 and α approach zero, then

$$\alpha^{4-i} \ln(1-e^{-\alpha})^{-1} \rightarrow 0$$

and so,

$$I_i \rightarrow \left(\frac{kT}{h}\right)^{5-i} (4-i)! \zeta(5-i),$$

where, ζ is the Riemann Zeta - Function. Then, since, $\zeta(4) = \pi^4/90$, therefore

$$I_1 \rightarrow \left(\frac{kT}{h}\right)^4 \frac{\pi^4}{15},$$

so that Eq.20 reduces to the familiar Stefan-Boltzmann law given by Eq. 16, where, $\sigma = 2\pi^5 k^4 / 15c^2 h^3$.

When ℓ is small, the integrals in Eq. 21 reduce to

$$I_i \approx \left(\frac{kT}{h}\right)^{5-i} [\alpha^{4-i} + (4-i)\alpha^{3-i} + (4-i)(3-i)\alpha^{2-i} + (4-i)(3-i)(2-i)]e^{-\alpha} \quad (22)$$

where, $i = 1, 2, 3$. When ℓ approaches zero, α becomes infinite so that $I_1 \rightarrow 0$. Now, since I_2/ℓ and I_3/ℓ^2 are proportional, respectively, to αI_2 and $\alpha^2 I_3$, therefore, both of these quantities approach zero, so that P , given by Eq.20, also approaches zero, as $\ell \rightarrow 0$.

Let P_a represent P in Eq. 20 when the integrals I_i are given by the approximate expressions in Eq. 22. Then, since, $\alpha = \text{constant}/\ell T$, it is easy to show that the error in P , given by $(P - P_a)/P$, is a function only of the product, ℓT . Fig. 17 shows a graph of this error versus ℓT . Note that the error approaches the asymptotic value of 0.076 as ℓT becomes large. Thus, the maximum error that can be incurred in P by employing Eq. 21 for the I_i is only 7.6 percent.

Values of the ratio, $P/\sigma T^4$, have been calculated as a function of ℓ for the temperatures $T = 300^\circ\text{K}$, 1000°K , 2000°K , where P is determined from Eq.21. The resulting curves are shown in Fig. 18. When $\ell < 100$ microns, note the significant departure of these curves from the classical Stefan-Boltzmann

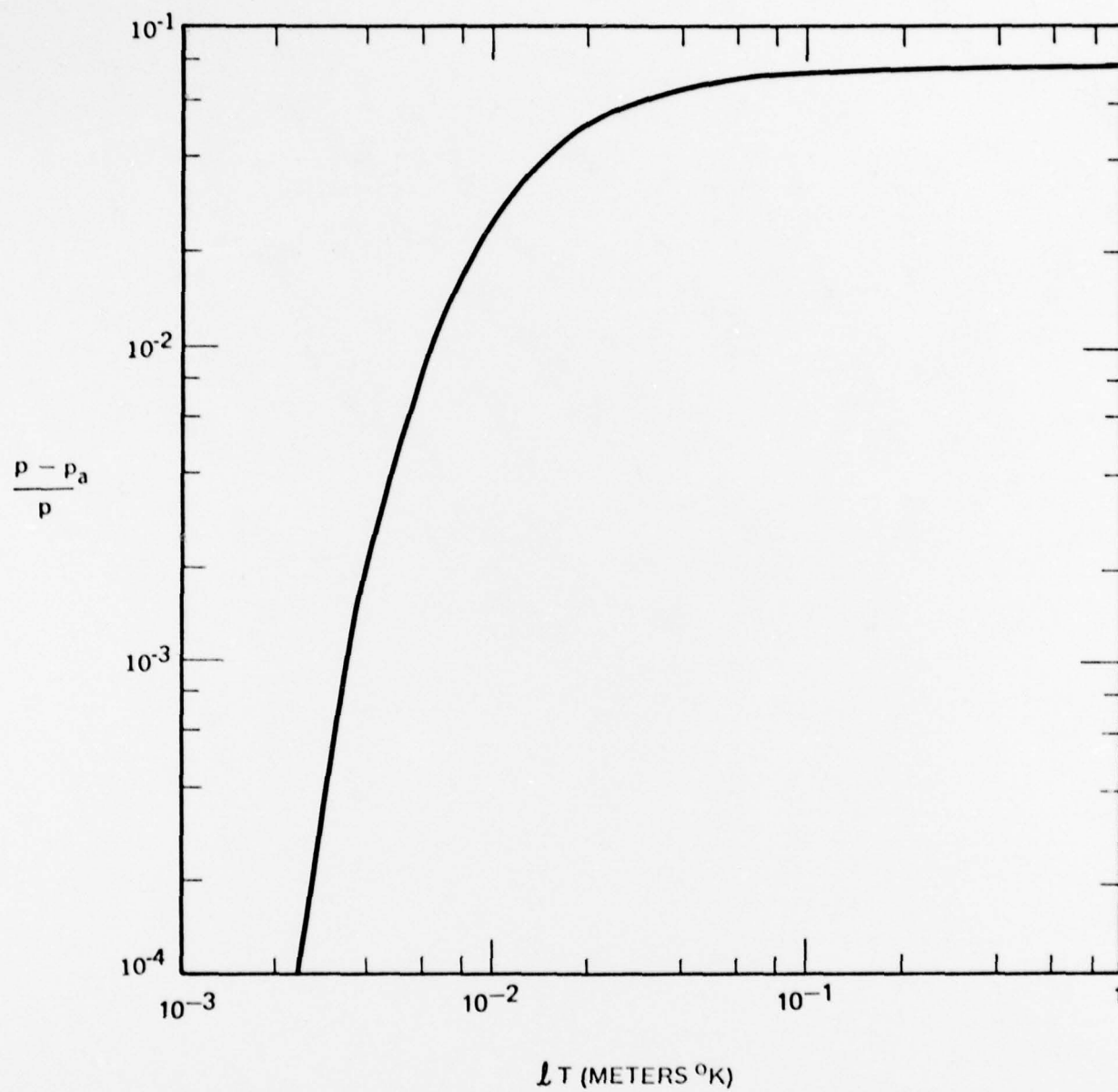


Figure 17 Error Incurred in p by Employing Eqs. (7) for the Integrals

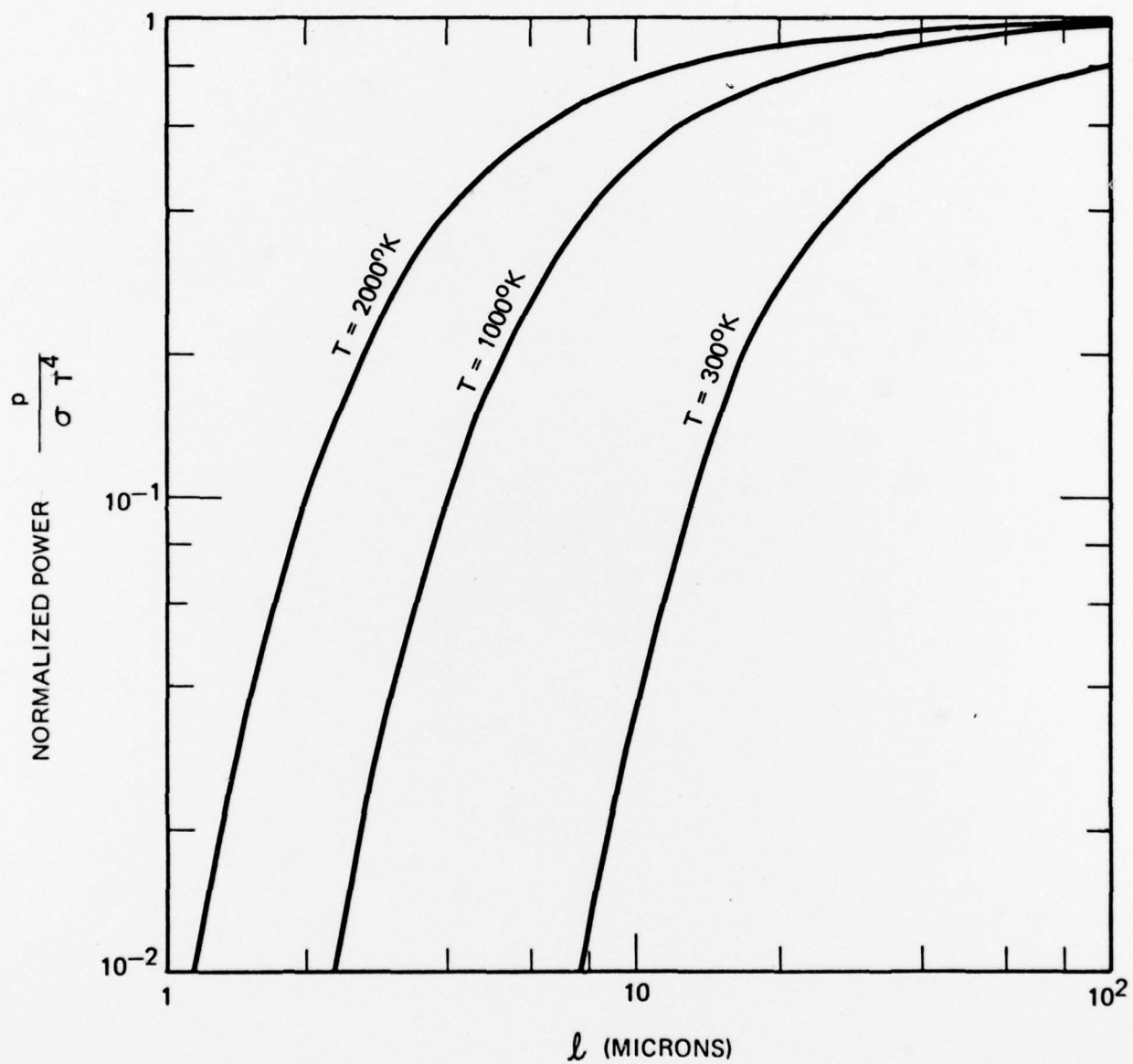


Figure 18 Normalized Power Per Unit Area Radiated from Cubical Blackbody versus Cube Edge, l

law, $P/\sigma T^4 = 1$. Thus, these curves imply that, at a given temperature, the power per unit area radiated by a cubical blackbody diminishes in magnitude as the size of the body decreases.

The decrease in P with decreasing values of ℓ has an interesting affect on the solidification time of a liquid metal. Consider a small metallic cube to be at its melting temperature, T . Assume that this cube radiates like a blackbody. Then, the solidification time, τ , of the cube is given by

$$\tau = \frac{\text{mass} \times H}{\text{area} \times P(\ell)} = \frac{\rho \ell^3 H}{6 \ell^2 P(\ell)} = \frac{\rho H}{6} \frac{\ell}{P(\ell)} \quad (23)$$

where, ρ and H are the density and heat of fusion, respectively, of the metal and $P(\ell)$ is given by Eq. 20 and 22. If ℓ is considerably larger than 100 microns and decreasing, $P(\ell)$ will remain constant and τ will also decrease. When ℓ drops below approximately 100 microns, $P(\ell)$ will no longer be constant but will vary with ℓ according to

$$P(\ell) = \left(\frac{A}{\ell^3} + \frac{B}{\ell^2} + \frac{C}{\ell} + D \right) e^{-K/\ell}$$

where, K, A, B, C, D are constants, and $K > 0$. Then, τ becomes

$$\tau = \frac{\rho H}{6} \frac{\ell^4 e^{K/\ell}}{A + B\ell + C\ell^2 + D\ell^3}.$$

As ℓ approaches zero, τ becomes infinite, since

$$\lim_{\ell \rightarrow 0} \ell^4 e^{K/\ell} \rightarrow \infty.$$

This means that τ decreases with decreasing values of ℓ until ℓ reaches a value which lies within an order of magnitude of 100 microns, and then τ begins to increase as ℓ continues to decrease, eventually becoming infinite as ℓ approaches zero. At present, this interesting behavior of τ is purely academic, since it has not yet been demonstrated in the laboratory.

2.5.2 HEAT LOSS SUFFERED BY INSULATED EHD SOURCE

One way of insulating the cylindrically shaped EHD source (shown in Fig. 1) against heat loss is to surround it with several thin, concentric, cylindrical heat shields made of molybdenum and separated by Saffil Alumina Fiber. The disadvantage of this particular scheme is the amount of time and effort expended in constructing the individual heat shields and then installing them, at equally spaced intervals, around the source. The greater the number of heat shields, the more time-consuming becomes the task.

A much simpler way of insulating the source is to cut a long, rectangular strip of molybdenum, - whose width coincides with the length of the source -, superimpose a thick layer of saffil alumina fiber on the molybdenum, and then wrap the long, thick, rectangular strip around the source, so that the molybdenum heat shield becomes a continuous spiral about the source. The disadvantage of this scheme, however, is that some of the heat from the source will be conducted away from the source along the continuous, spiral heat shield. This heat loss will, of course, be in addition to the heat lost by radiation. It is important to determine the magnitude of the conductive heat loss with the spiral shielding so that it can be compared with the radiative heat loss with the cylindrical shielding. If the former is negligible relative to the latter, then it will be advantageous to utilize the spiral technique of heat shielding.

An exact analytical description of the radiative heat loss for the spiral configuration is rather difficult to derive. However, this heat loss is expected to differ only slightly from pure radiative heat loss, since radiation in the radial direction must pass through the same number of heat shields in both configurations. Assume that the cylindrical heat shields and the surface of the cylindrical EHD source are gray, diffuse surfaces (a gray surface is one

whose emissivity is independent of temperature and wavelength). Also, assume that no heat is absorbed in the spaces between the heat shields. This is not a serious assumption, since the saffil alumina fiber is a reasonably good heat insulator. Let r_i denote the radius of the i^{th} heat shield, where, $i = 1, 2, \dots, n$, and where n = total number of heat shields, and let L = common length of the heat shields and the cylindrical source. Then the total net rate of heat loss, or, power loss, from a cylindrical configuration is

$$P_n = 2\pi r_n L \epsilon \sigma (T_n^4 - T_o^4) \quad (24)$$

where, P_n is the total net power radiated outward from the n^{th} , or, last, heat shield, T_n is the temperature of this heat shield and T_o is the known ambient temperature, i.e., the temperature of a heat shield having infinite radius. Also, ϵ = total hemispherical emissivity of the n^{th} shield, and σ = Stefan-Boltzmann constant = 5.67×10^{-8} watts/meter² °K⁴.

The only unknown quantity in Eq. 24 is T_n . However, in order to determine T_n , one must also determine the temperature of each of the n heat shields. Since the cylindrical surface of the source is also made of molybdenum, therefore, all of the cylindrical surfaces have the same total hemispherical emissivity, ϵ . Then, according to Reference 4, the total net power radiated outward from the source is

$$P_S = \frac{2\pi a L \epsilon \sigma (T_S^4 - T_1^4)}{1 + \frac{a}{r_1} (1-\epsilon)} \quad (25)$$

where, a = radius of the source, T_S = known temperature of the source, T_1 = unknown temperature of the first heat shield, and the net power radiated outward from the i^{th} heat shield is, similarly

$$P_i = \frac{2\pi r_i L \epsilon \sigma (T_i^4 - T_{i+1}^4)}{1 + \frac{r_i}{r_{i+1}} (1-\epsilon)} \quad (26)$$

where, $i = 1, 2, \dots, n-1$, and T_i = unknown temperature of the i^{th} heat shield. Eqs 24, 25, and 26 describe the net power radiated outward from the EHD source and the n heat shields. Since these equations describe the steady-state condition, therefore, the temperatures T_1, T_2, \dots, T_n are all constant. This means that the power incident on any given heat shield must equal the net power radiated outward from this same heat shield, otherwise its temperature would not remain constant. Thus, it follows that

$$P_S = P_1 = P_2 = \dots = P_{n-1} = P_n \quad (27)$$

so that the total net power radiated from a cylindrical configuration is given by either of the Eqs. 24, 25 and 26. However, in order to determine any one of the T_i , all n heat shield temperatures must be determined. This is done by solving the following n simultaneous equations for the n unknowns T_i :

$$P_S = P_1, P_1 = P_2, P_2 = P_3, \dots, P_{n-1} = P_n \quad (28)$$

where P_S is given by Eq. 25, P_1, P_2, \dots, P_{n-1} are given by Eq. 26, and P_n is given by Eq. 24.

For the EHD source, consider a total of $n = 8$ concentric, cylindrical heat shields, each of length $L = 4$ cm and having radii

$$r_{i+1} = r_i + 0.0844 \text{ cm}$$

where, $i = 1, 2, \dots, n-1$ and $r_1 = 1.5094$ cm. Also, $T_S = 1273^\circ\text{K}$ and $T_0 = 293^\circ\text{K}$. Finally, the radius of the source is $a = 1.425$ cm and the common emissivity is $\epsilon = 0.13$. Solving the eight simultaneous Eq. 28 for the eight heat shield temperatures yields:

$$\begin{array}{ll}
T_1 = 1225.8^\circ\text{K} & T_5 = 991.4^\circ\text{K} \\
T_2 = 1175.5^\circ\text{K} & T_6 = 908.2^\circ\text{K} \\
T_3 = 1121.0^\circ\text{K} & T_7 = 798.6^\circ\text{K} \\
T_4 = 1060.6^\circ\text{K} & T_8 = 616.6^\circ\text{K}
\end{array}$$

Then, by employing either of Eqs. 24, 25 or 26, the total net power radiated away from the cylindrical configuration, where $n = 8$, is (expressing all distances in meters)

$$P_T = 5.34 \text{ watts.} \quad (29)$$

As mentioned earlier, we shall assume that the above power is identical to that which would be radiated away from the spiral configuration, where the spiral contains a total of eight complete turns, and the distance between adjacent turns is 0.0844 cm.

We shall now calculate the conductive heat loss, or, power loss, through the continuous spiral which contains eight turns. The equation of the spiral is

$$r(\theta) = \frac{p}{2\pi} \theta + r_1 \quad (30)$$

where, (r, θ) are the polar coordinates of a point on the spiral and p = distance between adjacent turns = 0.0844 cm. The total length of the spiral is then

$$l = \int_0^{16\pi} r d\theta = \int_0^{16\pi} \left(\frac{p}{2\pi} \theta + r_1 \right) d\theta = 16\pi(4p + r_1) = 92.84 \text{ cm.}$$

We assume that the temperature at the end of the spiral closest to the source is equal to $T_1 (=1225.8^\circ\text{K})$ and that the temperature at the opposite end is equal to $T_8 (616.6^\circ\text{K})$. Then, assuming that the temperature varies linearly along the spiral, the power which is conducted along the spiral is given by

$$P_C = \frac{KA(T_1 - T_8)}{l}, \text{ watts} \quad (31)$$

where, K = thermal conductivity of molybdenum and A = cross-sectional area of the spiral = cross-sectional area of a heat shield = Lh , where, h = thickness of a heat shield. Here, $K = 146.5$ watts/meter $^{\circ}\text{K}$ and, $h = 2.54 \times 10^{-3}$ cm. Substituting in Eq. 31 then yields

$$P_C = 9.76 \times 10^{-2} \text{ watts.} \quad (32)$$

We note that P_C is only 1.83 percent of P_T , given by Eq. 29. Therefore, due to the relatively small value of the ratio P_C / P_T , it will be advantageous to thermally insulate the EHD source using the spiral configuration.

REFERENCES

1. H. Jones, Rep. Prog. Phys., 36, p. 1425-1497, 1973.
2. P. Ramachandrarao, M. G. Scott and G. A. Chadwick, Phil. Mag., 25, p. 961-982, 1972
3. P. G. Boswell and G. A. Chadwick, Scripta Metallurgica, 11, p. 459-465, 1977
4. Eshbach, O. W., Handbook of Engineering Fundamentals, 3rd edition, 1975; John Wiley and Sons; p. 1121.

SECTION 3

EXPANSION OF THE LABORATORY

Equipment composing a complete but small model machine shop was purchased and is operational. This includes a 10 inch Rockwell lathe, a Bridgeport mill, a metal band saw, a sander-grinder, and auxillary equipment and components. This equipment purchased with company funds allows for the in-house fabrication of most of the components and parts required for the research aspects of this program. Whenever commercial components are applicable and available, they will be used.

A new 1 ft. by 3 ft. vacuum chamber and test system is presently under fabrication. The system is very similar to the feasibility model and they will be able to use some of the power supplies and electronic instruments in common.

SECTION 4

SPECIAL EVENTS

Dr. P. Clarkin of ONR Washington visited the Phrasor Technology facility on 21 September and was briefed on the program accomplishments to date.

SECTION 5

PROBLEMS

No significant problems have been encountered that could affect the ultimate completion of the program goals, and the effort required to achieve the program objectives appears sufficient at the present time.

SECTION 6

FISCAL STATUS

(As of 31 October 1978)

Amount currently provided on contract	\$652,814
Expenditures and commitments to date	372,836
Funds required to complete work	279,978